Recycling of Proterozoic crust in Pleistocene juvenile magma and rapid formation of the Ok Tedi porphyry Cu–Au deposit, Papua New Guinea

M. van Dongen [a,*], R.F. Weinberg [a], A.G. Tomkins [a], R.A. Armstrong [b], J.D. Woodhead [c]

[a] School of Geosciences, PO BOX 28E, Monash University, 3800 VIC, Australia
[b] PRISE, Research School of Earth Sciences, Australian National University, Acton, 0200 ACT, Australia
[c] School of Earth Sciences, University of Melbourne, 3010 VIC, Australia

ARTICLE INFO

ABSTRACT

We present an investigation of the combined U–Pb, O and Hf isotope composition of zircons from a giant porphyry copper–gold deposit, hosted in a shoshonitic intermediate intrusive complex of the Ok Tedi area in Papua New Guinea. This area is part of a Late Miocene–Pliocene collisional fold-and-thrust belt related to island arc accretion to the Australian plate. Cathodoluminescence and transmitted light imaging reveal distinct zircon textures such as spongy rims and inherited zircon cores. Spongy textures, interpreted to result from corrosion of the surface by hydrothermal fluids, do not seem to affect the U–Pb, O and Hf isotope composition. Calculated SHRIMP U–Pb ages for the rims are 1.1–1.4 Ma whereas the inherited component is ~1.8 Ga. Our age results combined with existing K–Ar results, constrain the formation of the Ok Tedi deposit to <0.5 Myr. Oxygen isotope composition ($\delta^{18}O$), measured by SHRIMP, is ~6.5‰ for Pleistocene zircons but extend to values of ~8.3‰ or more for Proterozoic zircon cores. Likewise, corrected Hf isotope ratios from LA-ICP-MS analyses are centred on 0.2825 ($\varepsilon_{Hf(t)} = -6.5 \pm 2$) for Pleistocene zircons, compared to ~0.2815 ($\varepsilon_{Hf(t)} = +5$ to -3) for Proterozoic components. The Pleistocene zircon isotope signature is best explained by assimilation of Proterozoic crustal source material into asthenospheric mantle-derived magma similar to that of the Pliocene Porgera Au-only deposit in the same orogen.

© 2009 Elsevier B.V. All rights reserved.

1. Introduction

Our current thinking on how porphyry copper deposits form and evolve is firmly based on the orthomagmatic model (Sillitoe, 1972; Richards, 2003). In this model, hydrous intermediate to felsic magmas are emplaced in the upper 5 km of the crust, from which hydrothermal fluids exsolve and deposit copper and gold through fluid–rock interaction within the intrusion and the surrounding rocks. Often, these systems are characterised by multiple intrusive pulses, which can all be associated with fluid exsolution; a key to forming a hydrothermal ore deposit. However, there are numerous felsic hydrous magmas that have not formed deposits and there are many factors that contribute to the formation of an economic deposit.

In this paper, we investigate the duration of the process of ore deposition by constraining the timing of magmatism and we examine the origin of the magmas involved. The interpretation of radiometric ages of porphyry systems is problematic, since thermal pulses associated with multiple intrusions have the potential to reset grains (Seedorff et al., 2005), especially those of closure temperatures that are lower than felsic magmatic crystallisation temperatures, such as used in the Ar–Ar and K–Ar method.

We circumvent potential radiometric resetting and hydrothermal alteration problems by investigating the age and provenance of zircons, which are notably robust (Watson and Cherniak, 1997; Cherniak and Watson, 2001; Cherniak and Watson, 2003; Valley, 2003). We investigate zircon U–Pb isotope systematics, oxygen isotope and Hf isotope composition by SHRIMP and LA-ICP-MS analysis on samples from the Ok Tedi Cu–Au deposit. Our results show that the Ok Tedi magmatic rocks are extremely young and comprised of juvenile magmas and recycled material with a Proterozoic crustal signature.

2. Regional geology and samples

In this section, the geological background of this study is described, followed by a description of the sample set and their geological context.

2.1. Geological background

Collision of an island arc with the northern margin of the Australian craton, which forms the southern part of Papua New Guinea, resulted in the Papua New Guinean orogen, developed since the Early Miocene (Hill et al., 2002). The southern part of this east-west trending orogenic belt consists of a south-verging fold- and thrust-belt. The Ok Tedi Intrusive Complex is part of a discontinuous Pleistocene to recent magmatic belt of

---

* Corresponding author. Tel.: +61 7 3365 8248; fax: +61 7 3365 1277.
E-mail address: m.vandongen@uq.edu.au (M. van Dongen).

volcanic rocks and intermediate intrusions that form part of this thrust belt (Arnold and Griffin, 1978; Mason and McDonald, 1978; Housh and McMahon, 2000). The regional stratigraphy consists of shallowly dipping continental margin marine sedimentary rocks of Cretaceous to Middle Miocene age (Fig. 1). They overlie stable Palaeozoic metamorphic and granitic rocks of the West Papuan platform (Bamford, 1972).

The Ok Tedi deposit is one of the world's largest gold-rich porphyry copper deposits (PCDs) (Cooke et al., 2005). The Fubilan Monzonite Porphyry (FMP), which is the host to a large part of the Cu–Au mineralisation at Ok Tedi, is part of the larger calc-alkaline Ok Tedi Intrusive Complex (OTIC), which consists mainly of equigranular monzodiorite. The FMP is about 850 m in diameter and tapers downward. It intrudes surrounding sedimentary rocks and a slightly older monzodiorite stock, also part of the OTIC, which is referred to as the Sydney Monzodiorite (Rush and Seegers, 1990). Three-dimensional modelling of mine geology based on drill core indicates that the Sydney Monzodiorite is a subvertical tabular body, extending downward at least 700 m.

Field evidence for pre-, syn-, and post-emplacement slip motion along fault- and thrust planes, and skarn formation along these planes in the immediate vicinity of the deposit suggest a structural control on mineralisation (Van Dongen et al., 2008). The Ok Tedi intrusions occur in the hanging wall of a major thrust that connects to a deeper fault (Fig. 1)

thought to involve basement rocks (Mason, 1997; Hill et al., 2002). The FMP was emplaced into the relatively impermeable Ieru Siltstone that acted as a seal to mineralising fluids (Van Dongen et al., 2008) producing a typical porphyry-type, disseminated sulfide mineralisation in the FMP body itself. In contrast, a wedge of the Palaeogene Darai Limestone is in contact with the Sydney Monzodiorite at depth, which correlates with extensive endo- and exoskarn mineralisation along this contact, especially along breccias related to thrust planes, and potentially explains the lack of internal porphyry-style mineralisation. These zones of high strain and high permeability have played a major role in focussing mineralising fluids (Van Dongen et al., 2008).

The FMP and Sydney Monzodiorite are mineralogically and chemically nearly identical to the least altered phanerites of the OTIC, based on isocon diagram calculations (Doucette, 2000). These diagrams are used to calculate the effects of alteration and show that the differences in chemistry between the FMP and the neighbouring intrusions arise from extreme alteration caused by the hydrothermal event that produced the copper–gold mineralisation (Doucette, 2000). This is supported by changes in whole-rock geochemistry that correlate with alteration textures (Van Dongen et al., 2007).

The Ok Tedi ore consists of chalcopyrite, chalcocite, pyrite and minor bornite, deposited in quartz veins and stockworks in the central part of the FMP (Fig. 2). In addition, Au and Cu are found in disseminated
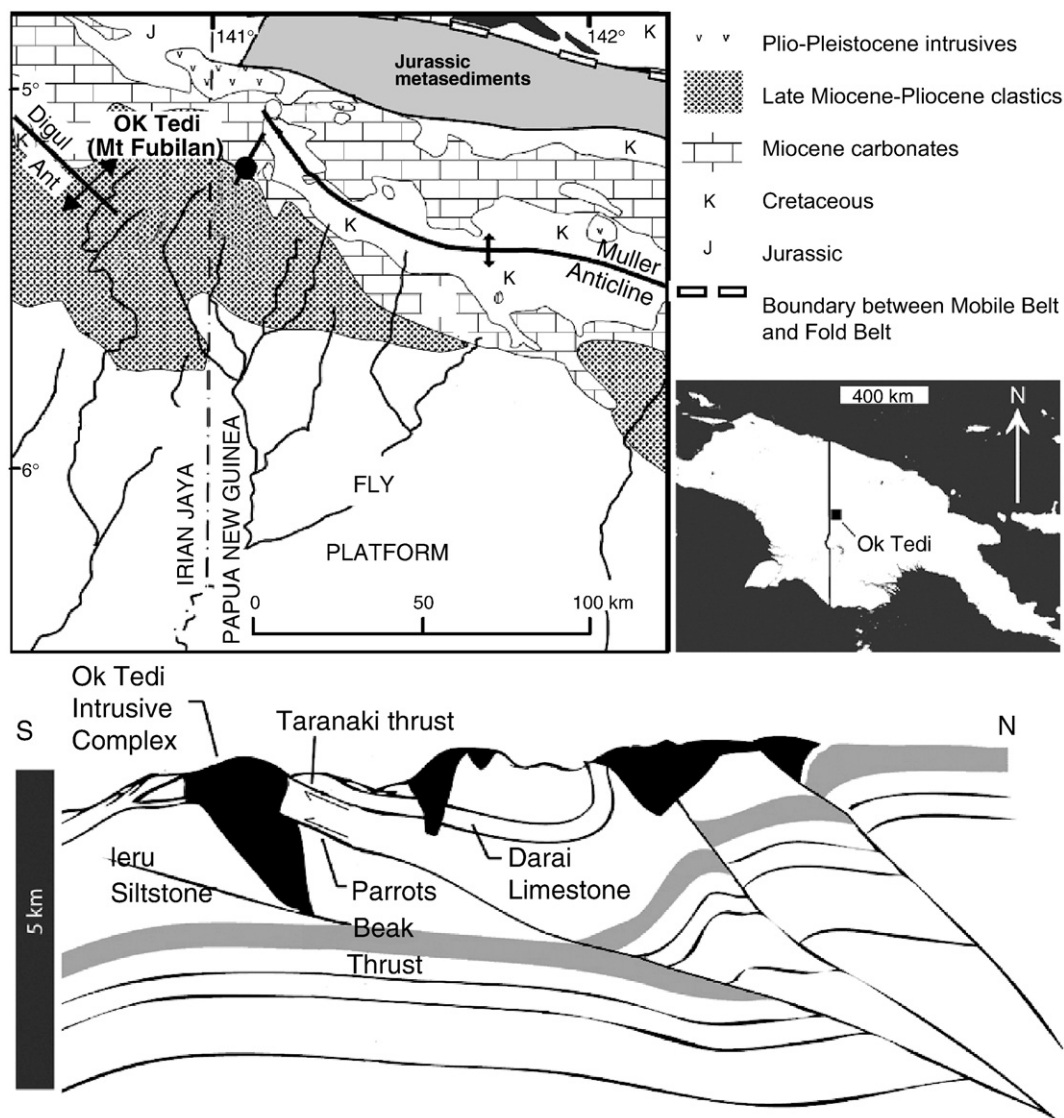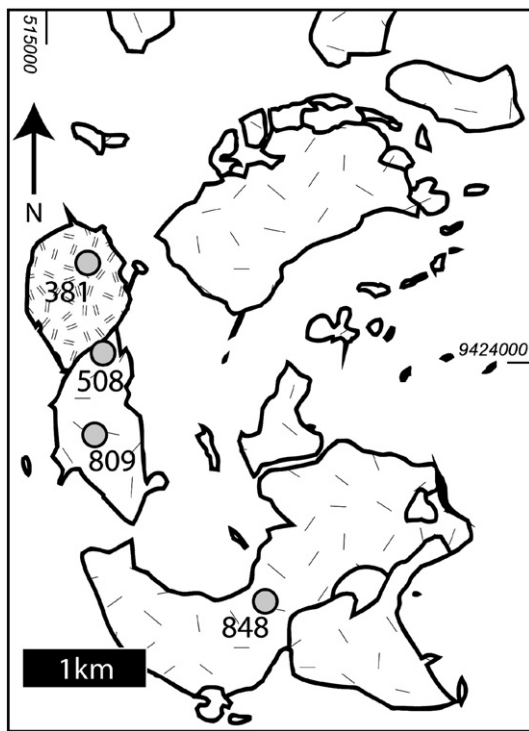

Fig. 1. Regional geology of the Ok Tedi deposit (modified from Hill et al., 2002) and geological cross section of the Ok Tedi deposit (modified from Mason, 1997).

Fig. 2. Ok Tedi intrusive complex with drill hole locations of samples. Legend: double dash fill = Fubilan Monzonite Porphyry, single dash = monzodiorite, including Sydney Monzodiorite. Coordinate grid is Australian Map Grid 1984.

sulfides in the monzonite stock and in massive magnetite and sulfide skarns in the immediate country rock. Hydrothermal activity has produced K–feldspar and biotite alteration spatially associated with the main Cu-bearing stockwork veins and disseminated chalcopyrite in the FMP, within a larger alteration zone characterised by disseminated pyrite and magnetite and minor chlorite and epidote. This propylitic alteration zone affects other intrusive stocks of the OTIC outside the mine area, though in varying intensity. Pseudomorphic replacement of mafic minerals (e.g. rhombs of chlorite–magnetite aggregates possibly after hornblende) is common. Calc-silicate alteration is spatially associated with massive magnetite and sulfide skarns, which forms carbonate replacement ore contrasting with the disseminated porphyry-type ore (Van Dongen et al., 2008).

The extensive alteration resulting from the hydrothermal event(s), which mineralised the Fubilan Monzonite Porphyry, was dated by K–Ar method on biotite and whole rock at 1.24–1.11 Ma (Page and McDougall, 1972; Page, 1975). Alteration has prevented obtaining a reliable crystallisation age for the emplacement of the FMP, as most Ar must have been from hydrothermal biotite and hornblende. Float samples from Harvey Creek, south of the Sydney Monzodiorite, resulted in an age of 2.6 ± 0.3 (2σ, in which σ = standard deviation) Ma by whole-rock K–Ar method, corrected for alteration effects (Page and McDougall, 1972). They were interpreted as representing the Sydney Monzodiorite, but this assumption is unsupported. It seems reasonable that most of the rocks of the OTIC are less than ~3 Myr old. In comparison, K–Ar analyses from samples from Mt Frew, Mt Anju and the Antares pluton, which lie within a 15 km radius of Ok Tedi, yielded ages between 7.2 ± 0.2 and 0.97 ± 0.06 Ma (Page, 1975). Assuming rapid cooling from the time of emplacement, this implies that the OTIC is one of the youngest exposed stocks from the Plio-Pleistocene magmatic belt that occurs on the southern side of the parallel-trending orogen.

2.2. Sample set

More than 40 different drill cores were inspected to verify the Ok Tedi Mining Limited in-house 3D geological model. The diamond drill hole locations of the samples used in this study (Fig. 2) were then chosen according to this model. Samples include one from the Fubilan Monzonite Porphyry (DDH 381–399 m), one from the Sydney Monzodiorite (DDH 809–116 m) and one monzodiorite sample from the southeast of the complex (DDH 848–417 m). Two other samples were from a drill hole at the contact between the two stocks. According to the 3D geological mine model, sample DDH 508–232 m corresponds to Fubilan Monzonite Porphyry, whereas the deeper sample DDH 508–366 m corresponds to Sydney Monzodiorite. This distinction is based on the degree of alteration (Table 1) rather than a clear distinction between the primary lithologies. Table 1 also shows that three of the samples are altered to a moderate extent, one is altered intensely (DDH 508–366 m) and one is weakly altered (DDH 848–417 m). Their mineral assemblages consist of varying amounts of plagioclase, K-feldspar and quartz, minor biotite, hornblende and diopside (or magnetite–biotite–sericite replacement, depending on alteration) and accessories are zircon, magnetite, chalcopyrite, apatite and occasionally titanite or rutile. Petrographic inspection shows that zircons occur within a variety of phase assemblages, e.g. within hydrothermal biotite and quartz aggregates, encapsulated by plagioclase, on K-feldspar groundmass grain boundaries and within fine-grained quartz.

3. Methods

Zircon grains were separated from the five samples (Table 1) following standard mineral separation procedures: crushing, milling, sieving, desliming, and heavy liquid and paramagnetic separation. Handpicked zircon crystals, which were distinctly pink, from 50 to 250 μm long, were mounted in epoxy together with chips of the Temora reference zircon, sectioned approximately in half and polished. Two mounts were produced: mount Z5137 contained zircons from DDH 508–232 m and 508–366 m; mount Z5158 contained zircons from the remaining three samples. Transmitted light and cathodoluminescence (CL) scanning electron microscope images were prepared for all samples. The images were used to target the SHRIMP beam onto single zircon growth zones. Zircon rims and inherited cores were both targeted. U–Pb analyses were carried out first. A subsequent analytical session was done to determine the oxygen isotope composition. The final analytical session consisted of measurement of the Hf isotope composition. Images were used to preferably target the same spots in the different sessions. Epoxy mounts were not polished in between analytical sessions.

U–Th–Pb analyses were made using the SHRIMP II at the Research School of Earth Sciences, Australian National University, following procedures in Ireland and Williams (2003) and references therein. Each analysis consisted of six scans through the mass range, with a Temora reference grain analysed for every three unknown analyses. The data were reduced using the SQUID Excel Macro of Ludwig (2001). U/Pb ratios were normalised relative to a value of 0.0668 for the Temora reference zircon, equivalent to an age of 417 Ma (Black et al., 2003).

The uncertainty in the U–Pb calibration is given per analytical session per individual mount. This uncertainty needs to be considered when comparing data from different mounts. Uncertainties given for individual analyses are at the 1σ level. Concordia plots (Tera and Wasserburg, 1972) and weighted mean $^{206}Pb/^{238}U$ and $^{207}Pb/^{206}Pb$ age calculations were carried out using ISOPLOT/EX (Ludwig, 2003). Weighted mean $^{206}Pb/^{238}U$ and $^{207}Pb/^{206}Pb$ ages were calculated and the uncertainties are reported as 95% confidence limits. Samples from within the mine area (only samples DDH 508–366 m and DDH 505–232 m) were subsequently analysed for oxygen and hafnium isotopes.

An important problem in U–Pb dating is how to correct for common Pb. For young zircons like those from Ok Tedi, the common Pb correction was made using ^{207}Pb, assuming that the analysis is concordant, i.e. that Pb/U has remained closed and that the $^{206}Pb/^{238}U$ – $^{207}Pb/^{235}U$ ages are the same. On our Tera-Wasserburg concordia plots the data were plotted uncorrected for common Pb. Hence the analyses

Table 1
Description of samples used for zircon separation.

Hole ID	Sample depth (m)	Di	Ttn	Hbl	Pl	Kfs	Qtz	Bt	Zrn	Mag	Ccp	Ms	Apt	Rt	A.I.	Mag. Text.	Alteration textures
DDH381	399				++	+	+	-	-	-				-	2	P	Selective–pervasive replacement of plagioclase by K-feldspar, mafic phenocrysts by biotite, most crystals full of fractures, K-feldspar-aggregates with corroded cores
DDH508	232				++	+	+	-	-					-	2	P	Selective–pervasive pseudomorphic replacement of feldspars and mafic phenocrysts, microcrystalline quartz and quartz infill
DDH508	366	–			++	+/+	+	/	-	/	-	-	-	-	3	P	Pervasive pseudomorphic replacement of feldspars and mafic phenocrysts, microcrystalline quartz and quartz infill
DDH809	116				+	+	+	-	-	-		-		-	2	P	Pervasive replacement by K-feldspar and biotite, especially of mafic enclaves, cryptocrystalline quartz matrix, incomplete quartz infill
DDH848	417	+		+	++			-	-	+	-			-	1	Eq	Selective magnetite and biotite replacement of mafic enclaves

Mineral abbreviations: Di = diopside, Ttn = titanite, Hbl = hornblende, Pl = plagioclase, Kfs = K-feldspar, Qtz = quartz, Bt = biotite, Zrn = zircon, Mag = magnetite, Ccp = chalcopyrite, Ms = muscovite, Apt = apatite, Rt = rutile. Abundances: – = sparsely present, - = present, / = common, + = abundant, ++ = dominant. A.I. = alteration index, in which 1 = fresh to weak, 2 = moderate, 3 = intense. Mag text = magmatic texture, in which P = porphyritic, Eq = equigranular.

plot along a line that intersects the *y*-axis (measured $^{207}Pb/^{206}Pb$) and the *x*-axis ($^{238}U/^{206}Pb$). This line is a mixture between the relevant common $^{207}Pb/^{206}Pb$ composition of the sample (model ratios based on Pb isotope models were used, e.g. Stacey and Kramers, 1975) and the radiogenic end-member (the lower intersection with the concordia curve). The lower the common Pb content, the closer the data point will plot to the lower axis. The age for each analysis is obtained by extrapolating each data point along the mixing line to the concordia and calculating a $^{206}Pb/^{238}U$ age from this composition.

SHRIMP II oxygen isotope analysis followed the methods described by Ickert et al. (2008). The internal standard used was the Temora II zircon with a $\delta^{18}O$ value of 8.2‰ (Black et al., 2004). The absolute accuracy achieved in measurements relative to a set of analyses of matrix-matched reference material is commonly ~1.0‰ (2 σ) or better. Oxygen isotope compositions were recalculated relative to Vienna Standard Mean Ocean Water and expressed as $\delta^{18}O$ (Craig, 1961). A confidence rating (Fig. 6) was constructed based on the presence of alteration features and inclusions at the analysed spots, using zircon photomicrographs. This rating is used for interpretation of magmatic features.

Hf isotope ratio determination was carried out by LA-MC-ICP-MS at the School of Earth Sciences, Melbourne University, following the method described in Woodhead et al. (2004). Zircons were ablated with a 193-nm ArF excimer laser, using a spot size of 55 µm, a 5 Hz repetition rate and laser fluence on the sample of <5 Jcm^{-2}. Total Hf beam signal intensity was between 5 and 12 V. Typical external uncertainty in the $^{176}Hf/^{177}Hf$ ratio was less than 0.00005 (2 σ).

For all zircons, ε_{Hf} was calculated using a Lu-Hf decay constant of 1.865×10^{-11} per year (Scherer et al., 2001) on the basis of the individual $^{238}U/^{206}Pb$ for Pleistocene age zircons and $^{207}Pb/^{206}Pb$ age for Proterozoic age zircons. ε_{Hf} was calculated following Kinny and Maas (2003):

$$\varepsilon_{Hf} = [(^{176}Hf/^{177}Hf_t)/(^{176}Hf/^{177}H_{CHUR})-1] \times 10000,$$

in which CHUR is the chondritic uniform reservoir and *t* is the time, indicated by the U–Pb age. Values used to calculate ε_{Hf} were $^{176}Hf/$

$^{177}Hf_{CHUR,t=0} = 0.282772$ (± 29) and $^{176}Lu/^{177}Hf_{CHUR,t=0} = 0.0332$ (± 2) (Blichert-Toft and Albarede, 1997). If the Hf ratio was measured on a zircon segment that was not directly dated by U–Pb, CL images were used to interpret the age of the segment, thus obtaining what is referred to as "inferred ages" in the figures. These ages are printed in italic in Table 3 because they introduce an uncertainty in the ε_{Hf} values due to potentially incorrect age assignment.

4. Results

This section is subdivided into three parts: description of zircon characteristics, results of U–Pb analysis and results of O and Hf isotope analysis.

4.1. Zircon imaging and characteristics

Features of the different zircon samples are described in Table 2. With the exception of sample DDH 848–417 m, most zircons have prismatic dipyramidal, euhedral crystal shapes and exhibit oscillatory zoning (Fig. 3), typical of magmatic zircons, with aspect ratios between 1:2 and 1:4. Roughly a third of the zircons from Ok Tedi contain inherited cores, identifiable by truncated zoning textures in CL. Roughly half of the zircons contain mineral inclusions and many contain melt inclusions. Notably, zircons from within the mine area can contain fluid inclusions, and can have spongy textures on the exterior parts of grains (Fig. 4), whereas both features are absent in sample DDH 848–417 m from outside the mine area. Most zircons identified in thin section were within plagioclase grains, although in altered samples (DDH 508–366 m), they may occur in aggregates of biotite and quartz (Table 2).

4.2. Zircon U–Pb ages

Zircon U–Pb analytical data are given in Appendix A. Ok Tedi zircon ages can be divided into a Pleistocene (<1.5 Ma) and a Proterozoic (>1.6 Ga) age group. Pleistocene ages (Fig. 5) vary between 1.12 ± 0.08 Ma (DDH

Table 2
Features of Ok Tedi zircons from cathodoluminescence (CL) and transmitted light (TL) image analysis.

Zircon sample	Aspect ratio	Contain distinct cores	CL texture	Shape	Min incl	Other incl	TL texture	Zircon association
508–232	1:2 to 1:4	19/59	Variable: osc, sec, few cloudy interiors	eu	23/59	m, minor f	Some broken, many healed cracks	N/a
508–366	1:2 to 1:4	13/54	Variable but mostly simple osc, some sec, few cloudy interiors	eu	24/54	f, m	Many spongy exteriors, many cracks	In cracked and altered Pl, in Bt-Qtz assemblage, in altered groundmass
381–399	1:2 to 1:4	15/52	Mostly osc, few cloudy interiors	eu	27/52	m, minor f	Some broken, some spongy exteriors	N/a
809–116	1:2 to 1:4	11/63	Mostly variable	eu	16/32	m	Occasional healed crack	In altered Pl
848–417	1:1	0/4	Few sec	eu	1/4		Angular, broken	In Pl

Abbreviations and signs used: / = out of a total of, osc = oscillatory zoning, sec = sector zoning, eu = euhedral, min incl = no. of zircons with mineral inclusions, m = melt inclusions, f = fluid inclusions, Bt = biotite, Qtz = quartz, Pl = plagioclase.
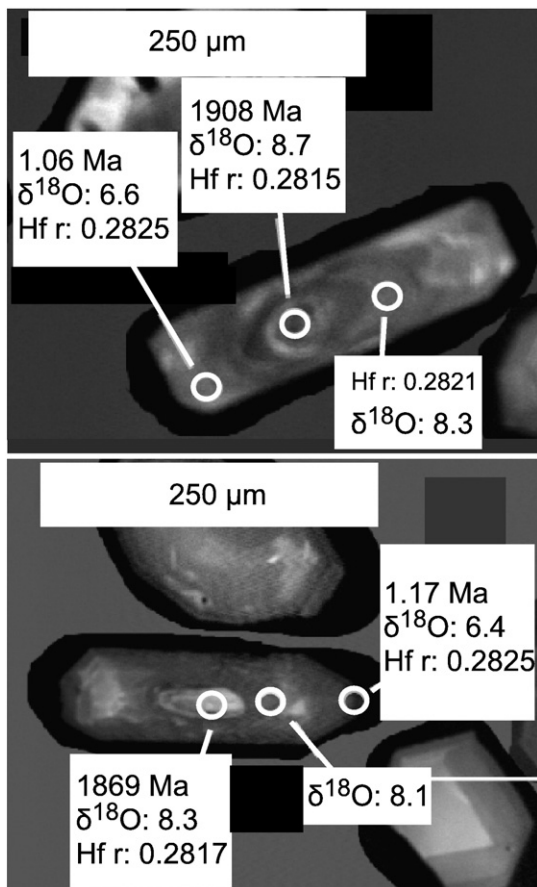
Fig. 3. Cathodoluminescence images of zircons from the Ok Tedi mine area. Circles indicate the analytical spot: ages calculated from U–Pb analysis, $\delta^{18}O$ and $^{176}Hf/^{177}Hf$ ratio (Hf r). Upper photograph shows typical zircon of sample DDH 508–232 m, lower photograph shows typical zircon from 508–366 m. Full image collection available in Appendix A.

508–366 m) and 1.43 ± 0.22 Ma (DDH 848–417 m). Error margins (2 σ error margins in the mean concordant ages of any of the samples do not warrant temporal distinction between them, except between DDH 508–366 m and DDH 848–417 m as these two are the only ones that do not have overlapping error margins. Proterozoic ages are discordant and have large associated errors in $^{206}Pb/^{238}Pb$ ages (Appendix A). $^{207}Pb/^{206}Pb$ ages are between 1.7 Ga and 2.1 Ga, predominantly between 1.8 and 1.9 Ga. The majority of Proterozoic ages are from zircon cores, but a few are from rims, e.g. DDH 508–232 O, DDH 508–366 B and G in Appendix A.

4.3. Zircon oxygen and hafnium isotope compositions

The results from SHRIMP $\delta^{18}O$ and LA-ICP-MS Hf isotope analysis are given in Table 3. Errors are reported as 2 σ. Oxygen isotope composition ($\delta^{18}O$) of Ok Tedi zircons varies between 5.0 ± 1 and 10.9 ± 1 without obvious correlation between isotope values and the presence of alteration features or inclusions (Fig. 6, Table 2).

The Hf isotope composition of Ok Tedi zircons (Table 2) can be divided into a large group of high $^{176}Hf/^{177}Hf$ at ~0.2825, and a smaller group of low $^{176}Hf/^{177}Hf$ at ~0.2815 (Fig. 7). The latter correlates with spots yielding Proterozoic ages (Table 2). In $\varepsilon_{Hf} - \delta^{18}O$ space the data defines distinct groups: a group of $\varepsilon_{Hf, 1.1 Ma} = -8 \pm 3$ and $\delta^{18}O = 6.5 \pm 1$ (Fig. 8 A), and a group of $\varepsilon_{Hf, 1.8 Ga} = -1 \pm 4$ and $\delta^{18}O = 8.3 \pm 1$ (Fig. 8 A). Errors in calculating ε_{Hf} values are discussed in Appendix A.

5. Discussion

Here we interpret the zircon textures, the zircon age dating results and what they imply for the duration of mineralisation and inheritance

of older zircons. We proceed to discuss and interpret the Hf and O results, and discuss their implications for magma source characterisation.

### 5.1. Interpretation of zircon textures

Most zircons have features typical of a magmatic origin, such as euhedral crystal shapes and oscillatory zoning (Corfu et al., 2003; Hoskin and Schaltegger, 2003). Therefore, we infer that the measured ages coincide with their magmatic crystallisation. However, there are some features that suggest an interaction with hydrothermal fluids, most notably spongy textures and fluid inclusions.

Spongy surfaces of zircons of the most altered sample (DDH 508–366 m, Table 1, Fig. 4 A) resemble textures from laboratory experiments in which zircons were exposed to hot acidic fluids (Geisler et al., 2003). In addition, many zircons from all samples, except DDH 848–419 m, contain randomly oriented fluid inclusion populations, sometimes close to cracks (Fig. 4 C). This suggests that some of the zircons in the altered samples interacted with hydrothermal fluids. We also found zircons within an alteration assemblage of K-feldspar and biotite, suggesting they might have formed as part of the hydrothermal assemblage (Nesbitt et al., 1999).

Most chemical features of zircons are indiscriminate between a hydrothermal and magmatic origin (Hoskin and Schaltegger, 2003) and textures alone do not discriminate unambiguously between hydrothermal and magmatic zircons either (Corfu et al., 2003). However, experimental work shows that hydrothermal alteration may change the composition of zircons when metamict domains are present (Geisler et al., 2003). Metamictisation is a key prerequisite for efficient isotopic re-equilibration of zircons in the presence of fluids (Balan et al., 2001; Geisler et al., 2007). The lack of metamict domains and similarity in U–Pb ages and oxygen isotope values between spongy-textured zircons and unaltered zircons (Fig. 6) suggest that hydrothermal alteration (e.g. Fig. 4 A) did not influence zircon isotopic composition at Ok Tedi. Therefore we interpret that zircons and their isotopic composition are the products of magmatic processes.

5.2. Duration of hydrothermal activity

Zircon ages of all samples centre around 1.16 ± 0.10 Ma suggesting that Ok Tedi is the youngest known giant Au-rich porphyry copper deposit exposed on Earth. This is probably due to the high erosion rates
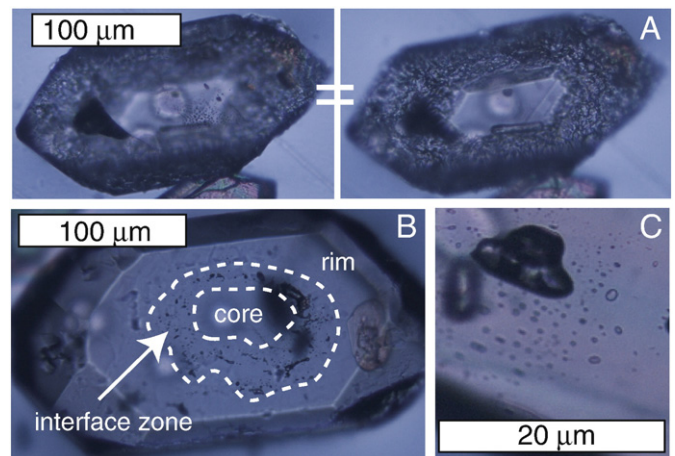
Fig. 4. Transmitted light images of typical zircons: A. From the most intensely altered sample DDH 508–366 m (Table 1), this shows the spongy texture at two depths in the zircon, indicating it is a feature of the surface of the zircon. This texture occurs in ~40% of zircon grains in this sample. B. Typical zircon from DDH 508–232 m. The stippled zone is the interface between core and rim, showing new zircon encapsulating micrometer-sized fragments, which are inferred to be remnants of inherited core after assimilation. C. Fluid inclusions in a zircon from DDH 508–232 m. The large dark blotch is interpreted as a partially recrystallised melt inclusion.
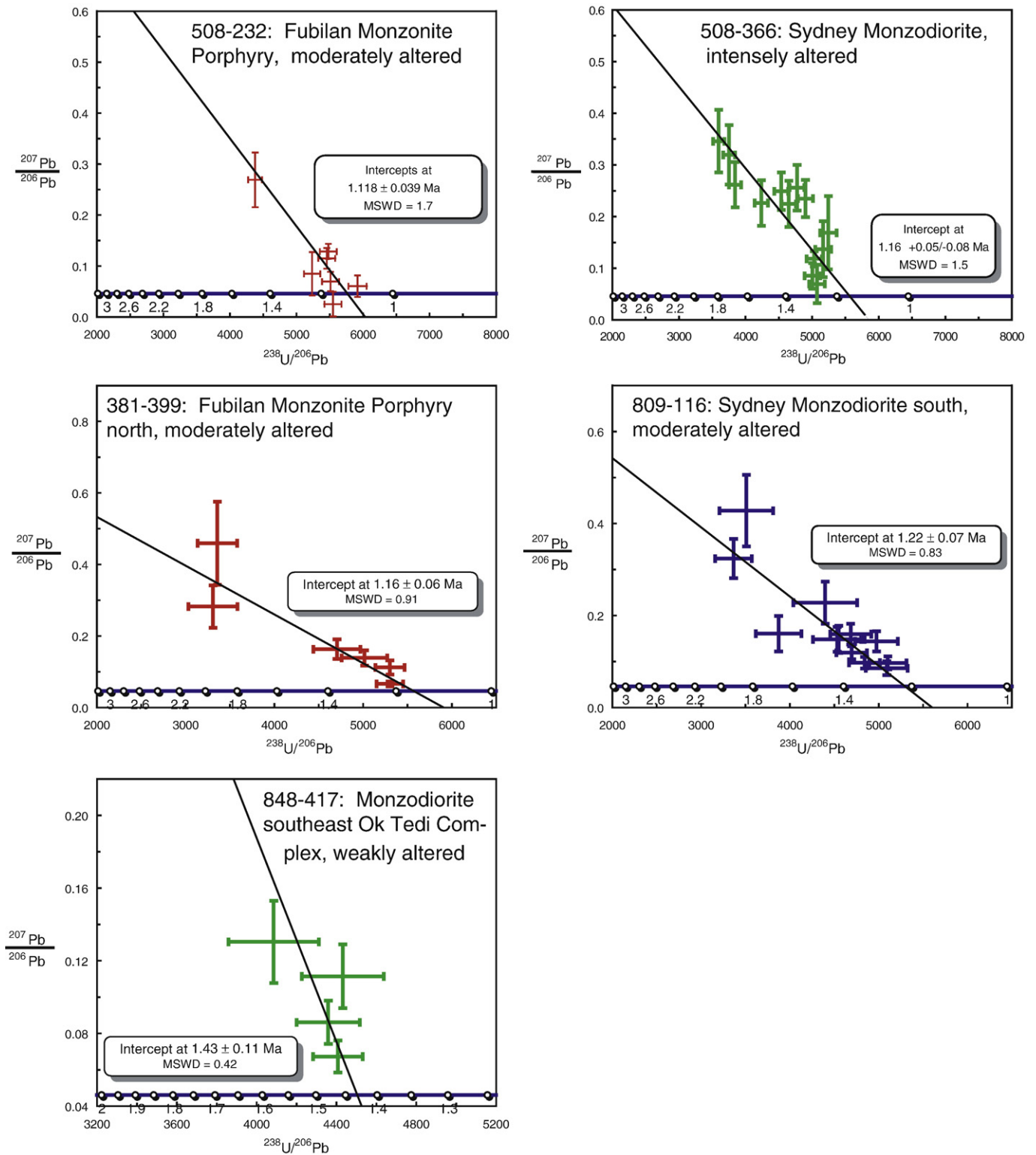
Fig. 5. Concordia diagrams of the five samples investigated, constructed from U–Pb isotopic composition of Ok Tedi zircons (detailed age data in Appendix A and Table 3). Error bars and calculated mean error are 1σ.

in Papua New Guinea (Weiland and Cloos, 1996), exposing the intrusion. This magma crystallisation age compares with an average K–Ar cooling age of 1.18 ± 0.05 Ma for in situ Fubilan samples (Page and McDougall, 1972) and ~2.6 Ma for the Harvey Creek float samples of uncertain origin (Page, 1975). Excepting the latter, our crystallisation ages are within error of the K–Ar ages (Page, 1975). Furthermore, similar zircon ages of

both the Sydney Monzodiorite and the Fubilan Monzonite Porphyry (Table 3) suggest that the two stocks most likely represent shallow expressions of the same magma, emplaced within error of the ages. The MSWD of 1.5 and 1.7 of samples DDH 508–232 and DDH 508–366 resp. (Fig. 5) indicates a scatter larger than expected from analytical error prediction, whereas the other three samples have smaller than expected

Table 3
SHRIMP II and LA-MC-ICP-MS analytical results of oxygen isotopes and Hf isotopes for Ok Tedi zircons from the mine area.

Sample DDH 508-232 m

CL image	Alt. feat.[a]	$\delta^{18}O$ value	Age corr. $^{176}Hf/^{177}Hf$	Age in Ma[b]	Initial Epsilon Hf
S	2	5.0	0.282540	1.08	−8.2
P	3	8.0	0.281562	*1883*	−0.8
P	2	9.4	0.281481	*1883*	−3.7
P	2	8.5	0.281543	*1883*	−1.5
P	3	8.5	0.281644	*1883*	2.1
R	3	7.0	0.282482	*1.11*	−10.2
R	2	7.1	0.282473	*1.11*	−10.6
R	3	6.5	0.282494	*1.11*	−9.8
Q	3	6.4	0.282560	1.22	−7.5
Q	2	6.5	0.282519	*1.22*	−8.9
O	3	9.1	0.281540	1851	−2.3
O	2	9.4	0.281512	1851	−3.3
	3	9.3	n.a.	1851	n.a.
K	2	6.3	0.281528	*1883*	−2.0
K	3	6.5	0.282689	1.22	−2.9
M	3	6.6	0.282600	1.00	−6.1
M	3	6.4	0.282546	1.14	−8.0
M	2	6.3	0.282547	1.14	−7.9
L	2	6.6	0.282621	1.04	−5.3
L		n.a.	n.a.	1734	n.a.
L	2	6.2	0.282364	1.04	−14.4
N	2	5.6	0.282448	1.50	−11.4
N		n.a.	0.282573	1.14	−7.0
J	2	7.3	0.281531	1858	−2.5
J	3	6.5	0.282567	1.12	−7.2
I	3	6.6	0.282548	0.99	−7.9
I	3	7.0	0.282497	*1.14*	−9.7
I	3	6.4	0.282531	0.99	−8.5
H	3	7.2	0.282515	*1.16*	−9.1
H	3	6.7	0.282510	*1.16*	−9.2
H	3	7.2	0.282619	*1.16*	−5.4
H	2	6.6	0.282514	*1.16*	−9.1
H	3	6.6	0.282493	*1.16*	−9.8
G	3	6.3	0.282520	*1.23*	−8.9
G	2	7.4	0.282542	*1.23*	−8.1
G	3	6.9	0.282586	*1.23*	−6.6
F	2	5.9	0.282566	*1.17*	−7.3
F	2	6.6	0.282590	*1.17*	−6.4
F	3	6.1	0.282546	1.17	−8.0
E	3	8.3	0.282146	1.06	−22.1
E	3	8.7	0.281542	1908	−1.0
E	3	6.6	0.282489	1.06	−10.0
D	3	6.0	0.282591	1.48	−6.4
D	3	6.9	0.282470	1.48	−10.7
D	3	6.5	0.282496	1.48	−9.7
D		n.a.	0.282590	1.48	−6.4
C	3	6.3	0.282622	*1.14*	−5.3
C	2	6.2	0.282647	*1.14*	−4.4
C	3	5.6	0.282573	1.07	−7.0
A	3	6.3	0.282146	*1.14*	−5.6
A	2	7.9	0.281625	2066	5.6
	3	7.9	n.a.	n.a.	n.a.
A	2	6.2	0.282214	*1.14*	−19.7
B	2	6.4	0.282452	1.3	−11.3
B	3	6.5	0.282562	*1.14*	−7.4

Sample DDH 508-366 m

CL image	Alt. feat.[a]	$\delta^{18}O$ value	Age corr. $^{176}Hf/^{177}Hf$	Age in Ma[b]	Initial Epsilon Hf
N	1	6.3	0.282618	1.08	−5.4
N	1	6.6	0.282600	*1.10*	−6.1
M	1	5.5	0.282632	1.13	−4.9
M	3	6.4	0.282638	*1.13*	−4.7
	1	5.6	n.a.	n.a.	n.a.
K	1	6.4	0.282547	1.06	−7.9
K	3	6.4	0.282479	*1.10*	−10.3
K	2	6.3	0.282515	1.50	−9.1
L	3	6.6	0.282558	1.48	−7.5
L		n.a.	0.282514	*1.10*	−9.1
J	1	6.5	0.281674	1869	2.8

Table 3 (*continued*)

Sample DDH 508-366 m

CL image	Alt. feat.[a]	$\delta^{18}O$ value	Age corr. $^{176}Hf/^{177}Hf$	Age in Ma[b]	Initial Epsilon Hf
J	2	8.3	0.282490	1.17	−9.9
	2	8.1	n.a.	n.a.	n.a.
I	3	8.1	0.281522	1846	−3.1
I	1	8.9	0.281572	*1846*	−1.3
	2	10.9	n.a.	*n.a.*	n.a.
F	2	9.2	0.281531	1843	−2.8
F	1	5.6	0.282180	*1.10*	−20.9
G	1	8.5	0.281778	1778	4.4
G	2	8.2	0.281556	*1840*	−3.4
H	1	6.6	0.282546	*1.19*	−8.0
H	2	6.9	0.282520	*1.19*	−8.9
D	1	8.3	0.281585	1846	−0.9
D	1	7.3	0.282513	1.07	−9.1
E	3	6.7	0.282615	*1.10*	−5.5
E	3	6.7	0.282560	1.37	−7.5
C		n.a.	0.281642	1955	3.7
C		n.a.	0.282309	*1.05*	−16.4
B		n.a.	0.281463	1743	−7.5
B		n.a.	0.281526	*1743*	−5.3
A		n.a.	0.282540	1.28	−8.2
A		n.a.	0.282517	*1.35*	−9.0
A		n.a.	0.282499	1.42	−9.6

Letters in column 1 refer to images of Appendix A to identify zircon grains. Alteration intensity for the oxygen isotope spots is listed as well. Column 2 contains subjectively determined alteration intensity based on cracks, fluid and mineral inclusions found under the optical microscope. Isotope analyses are given in column 3 and 4, age in Ma from SHRIMP U–Pb dating (see also Appendix A) is given in column 5. Calculated initial ε_{Hf} based on these ages is given in column 6.

[a] Presence of alteration features based on petrographic inspection, where 1 = many, 2 = few, 3 = none. See text and Fig. 6 for more detail.

[b] Age in Ma by SHRIMP U–Pb method, using $^{206}Pb/^{238}U$ age for Pleistocene ages, $^{207}Pb/^{206}Pb$ age for Proterozoic ages.

Ages in italic are inferred ages (as explained in the Methods section).

n.a. = not analysed or failed analysis.

scatter of data points. This is probably due to heterogeneity of the sample, e.g. not all zircons crystallised at exactly the same time.

Considering that the oldest zircon crystallisation age of DDH 848-417 is 1.43 ± 0.22 Ma and the youngest cooling age of biotite is 1.11 ± 0.05 Ma (Page and McDougall, 1972), the time span between early zircon crystallisation at ~800 °C cooling to ~350 °C is bracketed at ~0.5 Myr. This most likely brackets the duration of hydrothermal mineralisation from magmatic fluids as well, since it is likely that fluid exsolution starts at <650 °C (Lowenstern, 1994) and most of the copper was deposited before biotite alteration (Landtwing et al., 2005).

This short duration is comparable to results from other giant Au-rich porphyry copper deposit such as Grasberg (Pollard et al., 2005) and Bajo de la Alumbrera (Harris et al., 2004, 2008), estimated to have formed within ~1.7 Myr or less. Compared to several million years to form super giant porphyry copper deposits such as Chuquicamata (Ballard et al., 2001), this suggests a relationship between size and duration of magmatic activity. However, it also seems clear that giant deposits can form very rapidly given large amounts of enriched fluids. For example, it has been estimated that the Pleistocene Ladolam epithermal Au deposit on Lihir island in Papua New Guinea, which contains 1300 t Au, could have been formed in only 55 kyr, assuming 100% efficiency in the extraction of gold from currently active hydrothermal systems (Simmons and Brown, 2006). Thus, deposition efficiency and the time scales of mineralisation control deposit size.

5.3. Source of Proterozoic zircons

The resorbed cores of Proterozoic age (Table 3, Fig. 4 B) are evidence for assimilation of crustal rocks with a Proterozoic signature during Pleistocene magmatism. The Proterozoic ages obtained compare to felsic magmatic rocks on mainland northern Australia (Blewett et al., 1998). These could have supplied zircons directly to the Ok Tedi magma through
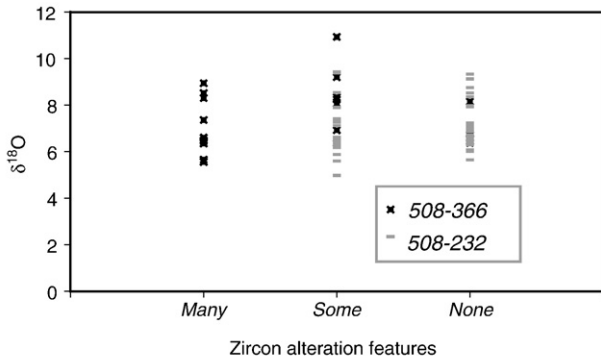
Fig. 6. Possible alteration features (cracks, fluid and mineral inclusions) in and around analytical spots show no correlation with oxygen isotope composition of zircons from DDH 508–232 m (grey dashes) and DDH 508–366 m (black crosses).

assimilation of crystalline basement underneath this part of Papua New Guinea, or indirectly through assimilation of sedimentary material derived from such granitic rocks and shed onto the northern passive margin of the Australian continent. Inherited zircons in porphyry copper deposit intrusions have been found in previous studies, e.g. Cornejo et al. (1997), Richards et al. (1999).

5.4. Oxygen isotopes

Mantle-derived magma typically has an oxygen isotope composition of 5.3 ± 0.3‰ (Valley, 2003), a value that is insensitive to magmatic differentiation (Valley et al., 2005). In contrast, zircons that have experienced interaction with crustal and atmospheric fluids, such as those found in sedimentary rocks and altered volcanic rocks, typically have higher values (Eiler, 2001; Hawkesworth and Kemp, 2006). Thus, $\delta^{18}O$ values above 5.6‰ in magmatic zircon indicate addition of a crustal oxygen isotope source to the magma from which the zircon precipitated.

The analytical results of zircons from Ok Tedi cannot be separated into different groups on the basis of the oxygen isotope composition alone. However, zircons of Proterozoic age have oxygen isotope values scattered around 8.3 ± 1‰ and zircons of Pleistocene age have oxygen isotope values scattered around 6.5 ± 1‰ (Fig. 7) with significant overlap between the two groups.

There are two possible interpretations of the data, depending on the relation between the inherited cores and the Pleistocene rims: 1) Proterozoic zircons were passive crystals of crustal origin that did not interact with Pleistocene magma. This implies that the assimilating Pleistocene magma was probably zircon saturated, of intermediate composition and of crustal origin in order to explain the O signature of the Pleistocene zircon rims, 2) Proterozoic supracrustal material, including zircons, was assimilated into zircon-undersaturated Pleistocene juvenile magmas, thus shifting the oxygen isotope value of newly precipitating zircons from 5.3 to the observed 6.5. We favour the second
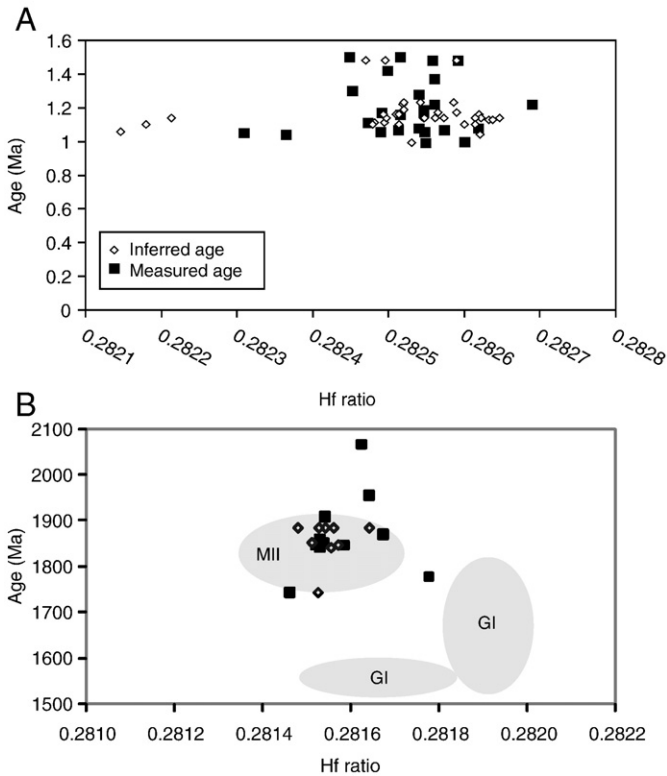
Fig. 7. SHRIMP U–Pb ages vs. LA-ICP-MS $^{176}Hf/^{177}Hf$ isotope ratio. Note difference in scale of the two plots: A. Plot for zircon grains or parts of grains with measured or inferred Pleistocene ages. B. Plot for zircon grains or parts of grains with measured or inferred Proterozoic ages. Zircons of same age range from Mt Surprise and Percyvale of the Georgetown Inlier ("GI") (Murgulov et al., 2007) and western Mt Isa Inlier ("MII") (Griffin et al., 2006; Bierlein et al., 2008) are shown in light grey shaded ovals for comparison. Pleistocene ages correspond to high Hf isotope ratios, with a few exceptions discussed in the text, whereas Proterozoic ages correspond to low Hf isotope ratios.
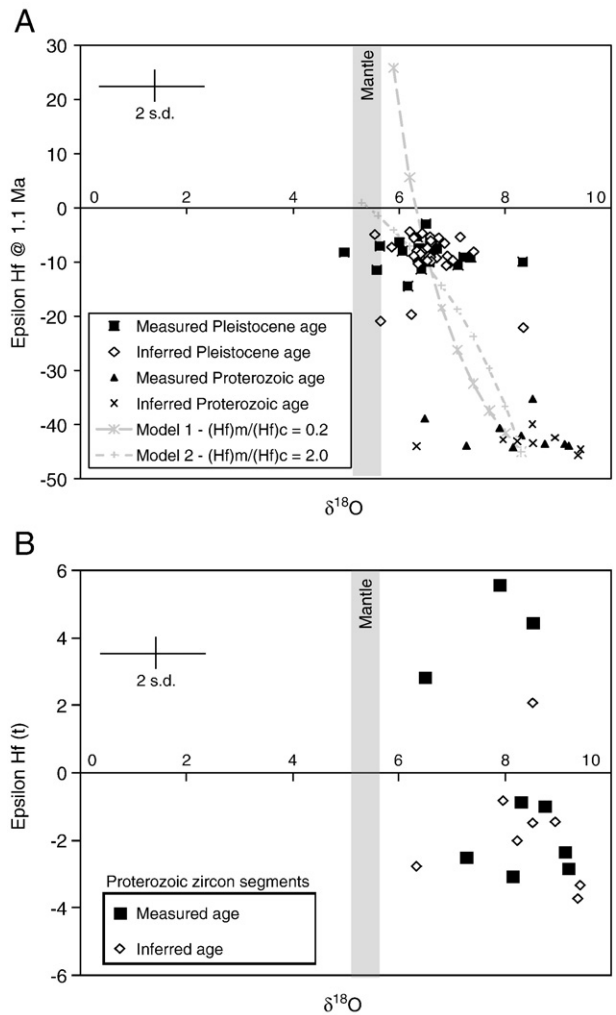
Fig. 8. Initial ε_{Hf} values vs. $\delta^{18}O$: A. Magmatic zircons with Pleistocene ages cluster around ε_{Hf} of -8.5 and $\delta^{18}O$ of 6.5. Those with Proterozoic ages cluster around ε_{Hf} of -40 and $\delta^{18}O$ of 8.3. Also shown are mixing model curves (dashed) between a crustal- and mantle-derived source, for two ratios of Hf concentration in the mantle vs. crust (0.2 and 2.0). More explanation in text. B. Proterozoic zircon spots (measured or inferred age). Initial ε_{Hf} (calculated for their individual ages) has values between -4 and 6, indicating both mantle and crustal sources for Proterozoic zircons.

scenario on the basis of: a) the corroded core texture of some inherited zircons (Fig. 4 B), b) the occurrence of 1.7 Ma gabbro within 5 km of the OTIC (Page, 1975) providing evidence for contemporaneous mafic magmatism, and more indirectly, c) the inferred importance of lower crust and mantle-derived magma in the genesis of Au-rich porphyry copper deposits (Hattori and Keith, 2001; Mungall, 2002).

5.5. Hafnium isotopes

The hafnium isotopic composition of zircons provides information about their magmatic source (Kinny and Maas, 2003). Lu is more compatible in mantle assemblages than Hf, which substitutes in zircon because of its similarity to Zr. ^{176}Lu decays to ^{176}Hf, thus enriching the depleted mantle in ^{176}Hf over time. Partial mantle melts therefore have a relatively radiogenic Hf isotope ratio relative to crustal melts formed at the same time. Because the isotope ratio changes over time, the epsilon (ε) notation is used to compare a particular Hf isotope ratio for a given time t, relative to the model isotope ratio for a uniform chondritic reservoir (CHUR). Thus, positive ε_{Hf} values indicate a relatively radiogenic, mantle-derived source, whereas negative values indicate a relatively unradiogenic, crustal source.

The zircon analyses of Ok Tedi samples have two distinct populations of Hf isotope ratios that correspond to the two U–Pb ages (Fig. 8, Appendix A). Pleistocene (~1.1 Ma) zircon components generally have ratios of ~0.2825 (s.d. 0.0000583, $\varepsilon_{Hf, 1.1 Ma} \sim -8.5 \pm 2$) whereas the majority of the Proterozoic (~1.9 Ga) zircon components have ratios of ~0.2815 ($\varepsilon_{Hf, 1.1 Ma} \sim -43 \pm 2$). Since the standard deviation of the relatively homogeneous Temora zircon standard (0.000044) is only slightly lower than that of the Pleistocene population, the composition of the latter may be considered statistically homogeneous, especially when considering that the Temora zircon contains a relatively high concentration of Hf. It is consistent with an interpretation of assimilation of Proterozoic crustal material by Pleistocene mantle-derived magma, provided that the assimilant was more heterogeneous in oxygen isotope composition than in Hf isotope composition.

Surprisingly, the large majority of detrital zircon Hf ratios from the Precambrian Georgetown Inlier in northeastern Australia (Murgulov et al., 2007), which is the closest terrane to Ok Tedi with known zircon Hf isotope ratios, does not show similar Hf ratios to Ok Tedi. Rather, the range in Proterozoic zircon Hf ratios from Ok Tedi compares closely with that of 1740–1900 Ma basement-derived zircons (Hf ratio 0.2814–0.2416) from the Mt Isa Inlier in northern Australia (Griffin et al., 2006; Bierlein et al., 2008), confirming our interpretation that Australian (possibly Mount Isa type) basement material, either directly or as erosion products, was incorporated into the magma that formed Ok Tedi. Unfortunately, the scatter of Proterozoic oxygen and hafnium isotope values (Fig. 8 B) and lack of obvious trends precludes a simple explanation for the origin of the Proterozoic zircon cores at this point.

5.6. Magma sources and assimilation

If Ok Tedi magmas resulted from mixing of a mantle-derived magma, which has a $\delta^{18}O$ of 5.3 (Valley, 2003), with a supracrustal $\delta^{18}O$ source of 8.3 (from Proterozoic cores), then to form zircons with $\delta^{18}O$ of 6.5 requires 40% assimilation of supracrustal material into the mafic melt. Analogous to AFC modelling of Kemp et al. (2007), we assume a mantle/crust Hf concentration ratio between 0.2 and 2. Assimilation of 40% Proterozoic crust (0.2815 Hf isotope ratio) by 60% mantle-derived melt to produce Ok Tedi zircons with a Hf isotope ratio of 0.2825 implies the Hf isotope ratio of the mantle-derived melt must lie above 0.2828 (Fig. 8 A). This is identical to present-day oceanic sediments and somewhat lower than present day MORB at 0.2831 (Chauvel et al., 2008). Since oceanic sediments have to be discounted as a source based on their high oxygen isotope value, our modelling results show that a mantle source for the hybrid magma may have been either lithospheric or asthenospheric mantle source. Since the

calculated mantle end-member with a Hf mantle/crust ratio of 2.0 would have an unlikely high Hf isotope ratio of 0.2860, we also infer that the Hf mantle/crust ratio in PNG is less than 2.0, hinting at asthenospheric mantle source such as was proposed for the genesis of the giant Grasberg Cu–Au deposit in Irian Jaya (Housh and McMahon, 2000). This is consistent with geodynamic models that invoke lithospheric delamination below the New Guinean orogen (Cloos et al., 2005).

The ~6 Ma alkali basalt of the Porgera gold deposit is the closest in time and space to the Ok Tedi deposit and the Sr, Nd, and Pb isotope composition indicates Porgera magmatic rocks are mantle-derived (Richards et al., 1990) and have not experienced crustal assimilation. We have used the Porgera basalt composition to back-calculate the composition of assimilated rock to produce the composition of our least altered, most primitive Ok Tedi monzodiorite. We have also calculated the effects of assimilation of typical Australian A-type granite (Turner et al., 1992) into the Porgera basalt to investigate whether it would produce a similar composition to the Ok Tedi monzodiorite.

Modelling results (Table 4) show that the assimilated rock necessary to modify the Porgera basalt to Ok Tedi monzodiorite should be composed largely of silica-, alumina- and alkali-oxides (i.e. probably a feldspar and quartz dominated rock) and that the hybrid magma would require subsequent fractionation of olivine, titanite and apatite, consistent with the crystallisation history suggested by Doucette (2000) based on whole-rock geochemistry and mineralogy. It also shows that the Porgera basalt, by assimilating typical A-type granite with 11.9 wt% Al_2O_3, would not reproduce the Ok Tedi intrusive rock with 18.7 wt% Al_2O_3. Considering the modelled bulk modal composition and the heterogeneity in the zircon isotope composition, the simplest explanation is that a sedimentary quartz–feldspar rock with 22.51 wt% Al_2O_3 was assimilated. More complex interpretations would require knowledge of zircon oxygen isotope composition of the proposed source regions.

The Hf isotope variations of the Ok Tedi zircons record the interaction between crustal and mantle sources in intermediate to felsic magma genesis (see also Chen et al., 2008; Murgulov et al., 2008; Peytcheva et al., 2008). Kemp et al. (2007) found ε_{Hf} values ranging from −10 to +10 and $\delta^{18}O$ values ranging from +5.5 to +9.5 in 415–390 Ma zircons from granite suites of the Lachlan Fold Belt (Australia) and Bolhar et al. (2008) found ε_{Hf} values of −4 to +12 and $\delta^{18}O$ values of 0 to 8‰ in 124–113 Ma zircons of granite suites from the western part of the South Island of New Zealand. Although both studies conclude that open system processes operated during magma evolution, they did not address the Hf-O isotopic composition of inherited zircons. The data from Ok Tedi samples, which suggests recycling of Palaeoproterozoic terrane with a signature similar to that of the Mt Isa terrane, shows that zircon core analysis may help to determine the nature of assimilated material.

Table 4
Major oxide values of: most primitive Porgera alkali basalt; the least altered most primitive sample of the Ok Tedi Complex; the crustal assimilant needed to produce the Ok Tedi sample composition after mixing 60% Porgera basalt with 40% crustal assimilant; a typical Australian A-type granite; and the mixture of 60% Porgera basalt with 40% typical Australian A-type granite.

	Primitive Porgera basalt P26	Most primitive Ok Tedi sample 871–199	Calculated crustal assimilant	A-type granite	Calculated granite basalt mix
Reference	Richards et al. (1990)	Van Dongen et al (in prep)		Turner et al. (1992)	
SiO_2	46.69	55.98	69.92	75.93	58.39
Al_2O_3	16.11	18.67	22.51	11.91	14.43
Fe_2O_3	9.65	6.90	2.78	1.93	6.56
MnO	0.21	0.13	0.00	0.07	0.15
MgO	9.09	2.24	−8.04	0.12	5.50
CaO	10.77	7.15	1.72	0.4	6.62
Na_2O	4.18	4.86	5.88	3.63	3.96
K_2O	1.22	2.91	5.45	4.5	2.53
TiO_2	1.38	0.79	−0.09	0.17	0.90
P_2O_5	0.68	0.35	−0.15	0.02	0.42

6. Conclusions

1) Zircons from samples of monzonite and monzodiorite from within the Ok Tedi mine area yielded SHRIMP U–Pb crystallisation ages within error of each other with an average of 1.16 ± 0.10 Ma, making it the youngest known giant porphyry copper–gold deposit on Earth.

2) Coincidence between zircon crystallisation age and K–Ar cooling age of hydrothermal biotite indicates that the process of mineralisation lasted less than ~0.5 Myr. This suggests that this giant ore deposit formed as a result of large volume flux rate of mineralising fluids.

3) Pleistocene zircons are characterised by a range of ε_{Hf} and $\delta^{18}O$ values (centred around -8 and 6.5, respectively) and include Proterozoic zircon cores (1.7–2.1 Ga) with a varied but crustal oxygen isotopic signature. Together the evidence suggests assimilation of a sedimentary package derived from a Proterozoic source by a (probably asthenospheric) mantle-derived magma.

4) Hf-O isotopic analysis of zircon cores constrains possible crustal sources that contribute to new zircon growth. Our results suggest assimilation of material with an isotopic signature similar to rocks from the Mt Isa terrane into the young magma that formed the Ok Tedi deposit.

Acknowledgements

Appendix A. Supplementary data

Supplementary data associated with this article can be found, in the online version, at doi:10.1016/j.lithos.2009.09.003.

References

Arnold, G.O., Griffin, T.J., 1978. Intrusions and porphyry copper prospects of the Star Mountains, Papua New Guinea. Economic Geology 73, 785–795.

Balan, E., Neuville, D.R., Trocellier, P., Fritsch, E., Muller, J.-P., Calas, G., 2001. Metamictization and chemical durability of detrital zircon. American Mineralogist 86 (9), 1025–1033.

Ballard, J.R., Palin, J.M., Williams, I.S., Campbell, I.H., Faunes, A., 2001. Two ages of porphyry intrusion resolved for the super-giant Chuquicamata copper deposit of northern Chile by ELA-ICP-MS and SHRIMP. Geology 29 (5), 383–386.

Bamford, R.W., 1972. The Mount Fubilan (Ok Tedi) porphyry copper deposit, territory of Papua and New Guinea. Economic Geology 67 (8), 1019–1033.

Bierlein, F.P., Black, L.P., Hergt, J., Mark, G.M., 2008. Evolution of Pre-1.8 Ga basement rocks in the western Mt Isa Inlier, northeastern Australia —insights from SHRIMP U–Pb dating and in-situ Lu–Hf analysis of zircons. Precambrian Research 163, 159–173.

Black, L.P., Kamo, S.L., Allen, C.M., Aleinikoff, J.N., Davis, D.W., Korsch, R.J., Foudoulis, C., 2003. TEMORA 1: a new zircon standard for Phanerozoic U–Pb geochronology. Chemical Geology 200, 155–170.

Black, L.P., Kamo, S.L., Allen, C.M., Davis, D.W., Aleinikoff, J.N., Valley, J.W., Mundil, R., Campbell, I.H., Korsch, R.J., Williams, I.S., Foudoulis, C., 2004. Improved Pb-206/U-218 microprobe geochronology by the monitoring of a trace-element-related matrix effect; SHRIMP, ID-TIMS, ELA-ICP-MS and oxygen isotope documentation for a series of zircon standards. Chemical Geology 205, 115–140.

Blewett, R.S., Black, L.P., Sun, S.S., Knutson, J., Hutton, L.J., Bain, J.H.C., 1998. U–Pb zircon and Sm–Nd geochronology of the Mesoproterozoic of North Queensland: implications for a Rodinian connection with the Belt supergroup of North America. Precambrian Research 89, 101–127.

Blichert-Toft, J., Albarede, F., 1997. The Lu–Hf isotope geochemistry of chondrites and the evolution of the mantle–crust system. Earth and Planetary Science Letters 148, 243–258.

Bolhar, R., Weaver, S.D., Whitehouse, M.J., Palin, J.M., Woodhead, J.D., Cole, J.W., 2008. Sources and evolution of arc magmas inferred from couple O and Hf isotope systematics of plutonic zircons from the Cretaceous Separation Point Suite (New Zealand). Earth and Planetary Science Letters 268, 312–324.

Chauvel, C., Lewin, E., Carpentier, M., Arndt, N.T., Marini, J.C., 2008. Role of recycled oceanic basalt and sediment in generating the Hf-Nd mantle array. Nature Geoscience 1 (1), 64–67.

Chen, B., Tian, W., Jahn, B.M., Chen, Z.C., 2008. Zircon SHRIMP U–Pb ages and in-situ Hf isotopic analysis for the Mesozoic intrusions in South Taihang, North China craton: evidence for hybridization between mantle-derived magmas and crustal components. Lithos 102, 118–137.

Cherniak, D.J., Watson, E.B., 2001. Pb diffusion in zircon. Chemical Geology 172, 5–24.

Cherniak, D.J., Watson, E.B., 2003. Diffusion in zircon. In: Hanchar, J.M., Hoskin, P.W.O. (Eds.), Reviews in Mineralogy & Geochemistry 53: Zircon. Mineralogical Society of America.

Cloos, M., Sapiie, B., Quarles van Ufford, A., Weiland, R.J., Warren, P.Q., McMahon, T.P., 2005. Special Paper 400: Collisional delamination in New Guinea : the geotectonics of subducting slab breakoff. Geological Society of America.

Cooke, D.R., Hollings, P., Walshe, J.L., 2005. Giant porphyry deposits: characteristics, distribution, and tectonic controls. Economic Geology 100 (5), 801–818.

Cornejo, P., Tosdal, R.M., Mpodozis, C., Tomlinson, A.J., Rivera, O., Fanning, C.M., 1997. El Salvador, Chile porphyry copper deposit revisited: geologic and geochronologic framework. International Geology Review 39 (1), 22–54.

Craig, H., 1961. Isotopic variations in meteoric waters. Science 133, 1833–1834.

Doucette, J.D., 2000. A petrochemical study of the Mount Fubilan Intrusion and associated ore bodies, Papua New Guinea. Ph.D. thesis, Oregon State University, Corvallis, 373p.

Eiler, J.M., 2001. Oxygen isotope variations of basaltic lavas and upper mantle rocks. In: Valley, J.W., Cole, D. (Eds.), Reviews in Mineralogy and Geochemistry 43: Stable isotope geochemistry. Mineralogical Society of America.

Geisler, T., Pidgeon, R.T., Kurtz, R., van Bronswijk, W., Schleicher, H., 2003. Experimental hydrothermal alteration of partially metamict zircon. American Mineralogist 88 (10), 1496–1513.

Geisler, T., Schaltegger, U., Tomaschek, F., 2007. Re-equilibration of zircon in aqueous fluids and melts. Elements 3 (1), 43–50.

Griffin, W.L., Belousova, E.A., Walters, S.G., O'Reilly, S.Y., 2006. Archaean and Proterozoic crustal evolution in the Eastern Succession of the Mt Isa district, Australia: U–Pb and Hf-isotope studies of detrital zircons. Australian Journal of Earth Sciences 53 (1), 125–149.

Harris, A.C., Allen, C.M., Bryan, S.E., Campbell, I.H., Holcombe, R.J., Palin, J.M., 2004. ELA-ICP-MS U–Pb zircon geochronology of regional volcanism hosting the Bajo de la Alumbrera Cu–Au deposit: implications for porphyry-related mineralization. Mineralium Deposita 39 (1), 46–67.

Harris, A.C., Dunlap, W.J., Reiners, P.W., Allen, C.M., Cooke, D.R., White, N.C., Campbell, I.H., Golding, S.D., 2008. Multimillion year thermal history of a porphyry copper deposit: application of U-Pb, Ar-40/Ar-39, (U-Th)/He chronometers, Bajo de la Alumbrera copper-gold deposit, Argentina. Mineralium Deposita 53 (3), 299–314.

Hattori, K., Keith, J.D., 2001. Contribution of mafic melt to porphyry copper mineralization: evidence from Mount Pinatubo, Philippines, and Bingham Canyon, Utah, USA. Mineralium Deposita 36 (8), 799–806.

Hawkesworth, C.J., Kemp, A.I.S., 2006. Using hafnium and oxygen isotopes in zircons to unravel the record of crustal evolution. Chemical Geology 226, 144–162.

Hill, K.C., Kendrick, R.D., Crowhurst, P.V., Gow, P.A., 2002. Copper–gold mineralisation in New Guinea: tectonics, lineaments, thermochronology and structure. Australian Journal of Earth Sciences 49 (4), 737–752.

Hoskin, P.W.O., Schaltegger, U., 2003. The composition of zircon and igneous and metamorphic petrogenesis. In: Hanchar, J.M., Hoskin, P.W.O. (Eds.), Reviews in Mineralogy & Geochemistry 53: Zircon. Mineralogical Society of America.

Housh, T., McMahon, T.P., 2000. Ancient isotopic characteristics of Neogene potassic magmatism in Western New Guinea (Irian Jaya, Indonesia). Lithos 50, 217–239.

Ickert, R.B., Hiess, J., Williams, I.S., Holden, P., Ireland, T.R., Lanc, P., Schram, N., Foster, J.J., Clement, S.W., 2008. Determining high precision, in situ, oxygen isotope ratios with a SHRIMP II: Analyses of MPI-DING silicate-glass reference materials and zircon from contrasting granites. Chemical Geology 257, 114–128.

Ireland, T.R., Williams, I.S., 2003. Considerations in zircon geochronology by SIMS. In: Hanchar, J.M., Hoskin, P.W.O. (Eds.), Reviews in Mineralogy & Geochemistry 53: Zircon. Mineralogical Society of America.

Kemp, A.I.S., Hawkesworth, C.J., Foster, G.L., Paterson, B.A., Woodhead, J.D., Hergt, J.M., Gray, C.M., Whitehouse, M.J., 2007. Magmatic and crustal differentiation history of granitic rocks from Hf-O isotopes in zircon. Science 315, 980–983.

Kinny, P.D., Maas, R., 2003. Lu-Hf and Sm-Nd isotope systems in zircon. In: Hanchar, J.M., Hoskin, P.W.O. (Eds.), Reviews in Mineralogy & Geochemistry 53: Zircon. Mineralogical Society of America.

Landtwing, M.R., Pettke, T., Halter, W.E., Heinrich, C.A., Redmond, P.B., Einaudi, M.T., Kunze, K., 2005. Copper deposition during quartz dissolution by cooling magmatic-hydrothermal fluids: the Bingham porphyry. Earth and Planetary Science Letters 235, 229–243.

Lowenstern, J.B., 1994. Dissolved volatile concentrations in an ore-forming magma. Geology 22 (10), 893–896.

Ludwig, K.R., 2001. SQUID 1.02, A User's Manual. Berkeley Geochronology Center Special Publication 2.

Ludwig, K.R., 2003. User's Manual for Isoplot/Ex, version 3.0, A Geochronological Toolkit for Microsoft Excel. Berkeley Geochronology Center Special Publication 4.

Mason, D.R., McDonald, J.A., 1978. Intrusive rocks and porphyry copper occurrences of Papua New Guinea – Solomon Islands region — reconnaissance study. Economic Geology 73, 857–877.

Mason, R.A., 1997. Structure of the Alice Anticline, Papua New Guinea: serial balanced cross-sections and their restoration. Journal of Structural Geology 19 (5), 719–734.

Mungall, J.E., 2002. Roasting the mantle; slab melting and the genesis of major Au and Au-rich Cu deposits. Geology 30 (10), 915–918.

Murgulov, V., Beyer, E., Griffin, W., O'Reilly, S.Y., Walters, S.G., Stephens, D., 2007. Crustal evolution in the Georgetown Inlier, North Queensland, Australia: a detrital zircon grain study. Chemical Geology 245, 198–218.

Murgulov, V., O'Reilly, S.Y., Griffin, T.J., Blevin, P.L., 2008. Magma sources and gold mineralisation in the Mount Leyshon and Tuckers Igneous Complexes, Queensland, Australia: U–Pb and Hf isotope evidence. Lithos 101, 281–307.

Nesbitt, R.W., Pascual, E., Fanning, C.M., Toscano, M., Saez, R., Almodovar, G.R., 1999. U–Pb dating of stockwork zircons from the eastern Iberian Pyrite Belt. Journal of the Geological Society 156 (1), 7–10.

Page, R.W., 1975. Geochronology of late Tertiary and Quaternary mineralized intrusive porphyries in the Star Mountains of Papua New Guinea and Irian Jaya. Economic Geology 70 (5), 928–936.

Page, R.W., McDougall, I., 1972. Ages of mineralization of gold and porphyry copper deposits in the New Guinea Highlands. Economic Geology 67 (8), 1034–1048.

Peytcheva, I., Von Quadt, A., Georgiev, N., Ivanov, Z., Heinrich, C.A., Frank, M., 2008. Combining trace-element compositions, U–Pb geochronology and Hf isotopes in zircons to unravel complex calcalkaline magma chambers in the Upper Cretaceous Srednogorie zone (Bulgaria). Lithos 104, 405–427.

Pollard, P.J., Taylor, R.G., Peters, L., 2005. Ages of intrusion, alteration, and mineralization at the Grasberg Cu–Au deposit, Papua, Indonesia. Economic Geology 100 (5), 1005–1020.

Richards, J.P., 2003. Tectono-magmatic precursors for porphyry Cu-(Mo–Au) deposit formation. Economic Geology 98 (8), 1515–1533.

Richards, J.P., Chappell, B.W., McCulloch, M.T., 1990. Intraplate-type magmatism in a continent-island-arc collision zone: Porgera intrusive complex, Papua New Guinea. Geology 18 (10), 958–961.

Richards, J.P., Noble, S.R., Pringle, M.S., 1999. A revised Late Eocene age for porphyry Cu magmatism in the Escondida area, northern Chile. Economic Geology 94 (8), 1231–1248.

Rush, P.M., Seegers, H.J., 1990. Ok Tedi copper-gold deposits. In: Hughes, F.E. (Ed.), Geology of the mineral deposits of Australia and Papua New Guinea, vol. 2. Australasian Institute of Mining and Metallurgy.

Scherer, E.E., Munker, C., Mezger, K., 2001. Calibration of the Lutetium–Hafnium clock. Science 293, 683–687.

Seedorff, E., Dilles, J.H., Proffett Jr, J.M., Einaudi, M.T., Zürcher, L., Stavast, W.J.A., Johnson, D.A., Barton, M.D., 2005. Porphyry deposits: characteristics and origin of hypogene features. In: Hedenquist, J.W., Thompson, J.F.H., Goldfarb, R.J., Richards, J.P. (Eds.), Economic Geology Hundredth Anniversary Volume. Society of Economic Geologists.

Sillitoe, R.H., 1972. A plate tectonic model for the origin of porphyry copper deposits. Economic Geology 67 (2), 184–197.

Simmons, S.F., Brown, K.L., 2006. Gold in magmatic hydrothermal solutions and the rapid formation of a giant ore deposit. Science 314 (5797), 288–291.

Stacey, J.S., Kramers, J.D., 1975. Approximation of terrestrial lead isotope evolution by a two-stage model. Earth and Planetary Science Letters 26, 207–221.

Tera, F., Wasserburg, G.J., 1972. U-Th-Pb systematics in 3 Apollo 14 basalts and problem of initial Pb in lunar rocks. Earth and Planetary Science Letters 14 (3), 281–304.

Turner, S.P., Foden, J.D., Morrison, R.S., 1992. Derivation of some A-type magmas by fractionation of basaltic magma — an example from the Padthaway Ridge, South Australia. Lithos 28 (2), 151–179.

Valley, J.W., 2003. Oxygen isotopes in zircon. In: Hanchar, J.M., Hoskin, P.W.O. (Eds.), Reviews in Mineralogy & Geochemistry 53: Zircon. Mineralogical Society of America.

Valley, J.W., Lackey, J.S., Cavosie, A.J., Clechenko, C.C., Spicuzza, M.J., Basei, M.A.S., Bindeman, I.N., Ferreira, V.P., Sial, A.N., King, E.M., Peck, W.H., Sinha, A.K., Wei, C.S., 2005. 4.4 billion years of crustal maturation: oxygen isotope ratios of magmatic zircon. Contributions to Mineralogy and Petrology 150 (6), 561–580.

Van Dongen, M., Tomkins, A.G., Weinberg, R.F., 2007. Trace element remobilization at the Ok Tedi Cu–Au deposit. Papua New Guinea. Proceedings of the ninth biennial meeting of the society for geology applied to mineral deposits, Irish Association for Economic Geology.

Van Dongen, M., Weinberg, R.F., Tomkins, A.G., Armstrong, R.A., 2008. Timescale of forming a giant porphyry Cu–Au deposit — Ok Tedi, Papua New Guinea. Proceedings of the Pacrim Congress, Gold Coast, Australia. Australasian Institute of Mining and Metallurgy.

Watson, E.B., Cherniak, D.J., 1997. Oxygen diffusion in zircon. Earth and Planetary Science Letters 148, 527–544.

Weiland, R.J., Cloos, M., 1996. Pliocene–Pleistocene asymmetric unroofing of the Irian fold belt, Irian Jaya, Indonesia: apatite fission-track thermochronology. Geological Society of America Bulletin 108 (11), 1438–1449.

Woodhead, J., Hergt, J., Shelley, M., Eggins, S., Kemp, R., 2004. Zircon Hf-isotope analysis with an excimer laser, depth profiling, ablation of complex geometries, and concomitant age estimation. Chemical Geology 209, 121–135.